Integration hydrogen evolution and water-cleaning via robust graphene supported noble-metal-free $Fe_{1-x}Co_xS_2$ system

Yingying Fan,[a,b] Dandan Wang,[a] Dongxue Han,[a*] Yingming Ma,[a] Shuang Ni,[a] Zhonghui Sun,[a,b] Xiandui Dong,[a] Li Niu[a,c]

[a] *State Key Laboratory of Electroanalytical Chemistry, c/o Engineering Laboratory for Modern Analytical Techniques, CAS Center for Excellence in Nanoscience, Changchun Institute of Applied Chemistry, Chinese Academy of Sciences, Changchun, 130022, P. R. China.*

[b] *University of Chinese Academy of Sciences, Beijing, 100049, P. R. China.*

c School of Chemistry & Chemical Engineering, Linyi University, Linyi 276005, P. R. China.

Experimental Section

Materials: Cobalt (II) acetate ($C_4H_6O_4$•Co•$_4H_2O$) was obtained from Sigma-Aldrich. Thioacetamide (TAA) was received from J&K Scientific. Iron (III) nitrate ($Fe(NO_3)_3$•$9H_2O$) and graphite powder (99.9 %, 325 mesh) were both purchased from Beijing Chemical Factory (Beijing, China). N, N - dimethylformamide (DMF, AR) was got from Fuyu Chemical Reagent. Deionized water with a resistivity of 18.2 MΩ cm was used for aqueous solutions. Graphene oxide (GO) was prepared by a modified Hummer methods.

Synthesis of Co-doped FeS_2/RGO composite: 0.13 g Iron (III) nitrate, a series of Cobalt (II) acetate (0.003g, 0.006g, 0.009g, 0.012g and 0.03g) were dissolved in 1.2 mL deionized water to form solution A, 0.3 g TAA dispersed in 4 mL deionized water to form solution B. Then, both solution A and B were added into 16 mL DMF solution. In addition, 0.6 mL 3 mg mL^{-1} graphene oxide aqueous solution was injected to the above solution with constant stirring. The mixture was put into a 90^{o}C oil bath for 24 h without reflux apparatus. The production was centrifuged and washed with deionized water for three times. Then the precipitant was dispersed again into 16 DMF solution following with a solvothermal process at 180 ^{o}C for 5 h to promote the degree of crystallinity.

Synthesis of $Fe_{0.86}Co_{0.14}S_2$: 0.13 g Iron (III) nitrate and 0.009 g Cobalt (II) acetate were dissolved in 1.2 mL deionized water to form solution A, 0.3 g TAA dispersed in 4 mL deionized water to form solution B. Both solution A and B were added into 16 mL DMF solution. The mixture was put into a 90 ^{o}C oil bath for 24 h without reflux apparatus. The production was centrifuged and washed with deionized water for three times. Then the precipitant was dispersed again into 16 DMF solution following with a solvothermal process at 180 ^{o}C for 5 h to promote the degree of crystallinity.

Synthesis of FeS_2/RGO: The relevant synthesized process is similar to that of Co-doped FeS_2/RGO composite, except the introduction of Cobalt (II) acetate.

Synthesis of FeS_2: The relevant synthesized process is similar to that of FeS_2/RGO composite, except the introduction of RGO.

Characterizations

Powder XRD data was acquired using a D8 Focus diffractometer (Bruker) with Cu Kα radiation (λ = 0.15405 nm). The Field - emission scanning electron microscope (FESEM) illustrations, High-angle annular dark - field scanning transmission electron microscopy (HAADF - STEM) and corresponding element mapping images were carried out on FE-SEM (Philips XL30 ESEM-FEG integrated with a EDAX system). Transmission electron microscopy (TEM) was carried out on a Tecnai G2 microscope operating at 200 kV. X-ray photoelectron spectroscopy (XPS) was performed at an ESCALAB MKII X-ray photoelectron spectrometer by monochromated Al Kα X-rays.

Electrochemical Measurements

The HER performance tests were carried out in a three-electrode system. The catalyst deposited on a glassy carbon electrode (GCE) was used as working electrode, a saturated calomel electrode (SCE) as the reference electrode and a graphite rod as counter electrode. The measured potential referencing SCE was further calibrated to reversible hydrogen electrode (RHE). Typically, 5 mg catalyst samples were dispersed into 1mL ethanol/water solution (ethanol/water = 1: 1) with 10 μL 5 wt % Nafion solution to form catalyst ink. 10 μL catalyst ink was deposited on GCE with 3 mm in diameter. Linear sweep voltammetry of HER was conducted at a scan rate of 5 mV s^{-1} for the polarization in the mixed solution of 0.5 M H_2SO_4 and 5 mg L^{-1} methyl orange (MO) with iR correction. Linear sweep voltammetry (LSV) of oxygen evolution reaction (OER) was conducted at a scan rate of 5 mV s^{-1} for the polarization in 0.5 M H_2SO_4 and the mixed solution of 0.5 M H_2SO_4 and 5 mg L^{-1} methyl orange (MO) respectively. Cyclic voltammetry (CV) curves were measured at a scan rate of 100 mV s^{-1} for 1000 cycles in a solution of 0.5 M H_2SO_4 without iR correction. LSV and CV curves were both performed on a CHI760e electrochemical analyzer (CH Instruments, Inc., Shanghai). Combination curves of time-dependent current density on cathode and the degradation potential on anode of MO degradation process were measured on a DC-EC-2.0 electrochemical analyzer (DyneChem, Changchun)with certain circuit transformation. Electrochemical impedance spectroscopy (EIS) measurements were carried out with a Solartron 1255B Frequency Response Analyzer (Solartron Inc., U.K.) with frequencies ranging from 100 kHz to 0.01 Hz. Ultraviolet visible (UV-Vis) absorptions were obtained using a Hitachi U-3900 spectrometer.

In addition, the acidic organic waste simulated by laboratory (0.5 M H_2SO_4 + 5 mg L^{-1} methylene blue, 0.5 M H_2SO_4 + 5 mg L^{-1} Rhodamin B) and the actual industry wastewater were also investigated by the methods mentioned above.

Computational details

Our theoretical calculations are spin-polarized calculations based on DFT within the Perdew-Burke-Ernzerhof (PBE) generalized gradient approximation and the projected augmented wave (PAW) method as implemented in the Vienna ab initio simulation package (VASP). To describe the lattice constants accurately, the PBE+U method was used with U_{Fe}= 2 eV for Fe d-orbitals and U_{Co}= 3.3 eV for Co d-orbitals. The cutoff energy for the plane-wave basis set is 350 eV and the Brillouin zone is sampled with the k-point separation < 0.04 Å-1. For the structure optimization, all the atomic positions except the bottom 9 atomic layers are relaxed until their residual forces are less than 0.03 eV Å-1. The FeS_2 (100) surface is considered because of its lowest surface energy. In this work, we investigated the H adsorption energy towards a (2×2) FeS_2 (100) surface supercell consisting of 6 atomic Fe monolayers, 12 atomic S monolayers as well as 15 Å vacuum on the top. One and three of the eight Fe atoms on the top layer have been replaced by Co atoms to study surface doping with Co content of 12.5% and 37.5%, respectively. The adsorption energies are calculated following the equation $E_{ads} = E_{H/surface}-(E_H+E_{surface})$, where $E_{H/surface}$, E_H, and $E_{surface}$ are the total energies of the surface with absorbent of H atom, the isolated H atom and the surface without absorbent, respectively.

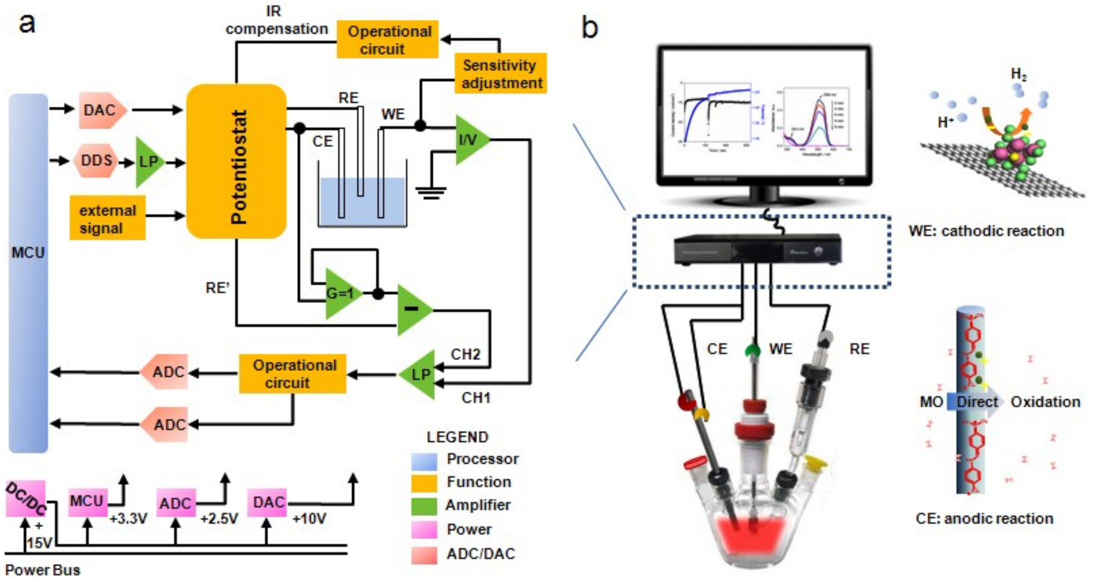

Figure S1. The corresponding modified circuit diagram illustration of the innovative electrochemical workstation. The WE measurement was a virtual ground mode and the CE need an Op-amp buffer.

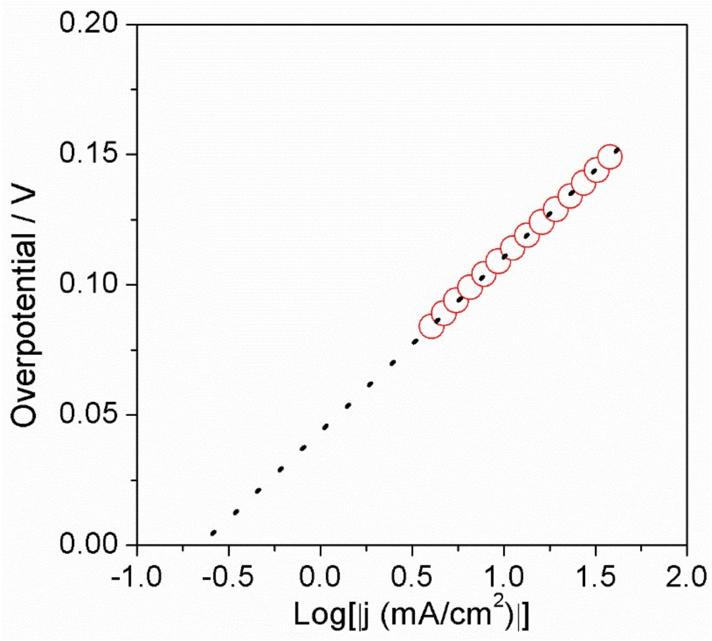

Figure S2. Calculated exchange current density of Fe$_{0.86}$Co$_{0.14}$S$_2$/RGO by applying extrapolation method to the Tafel plot.

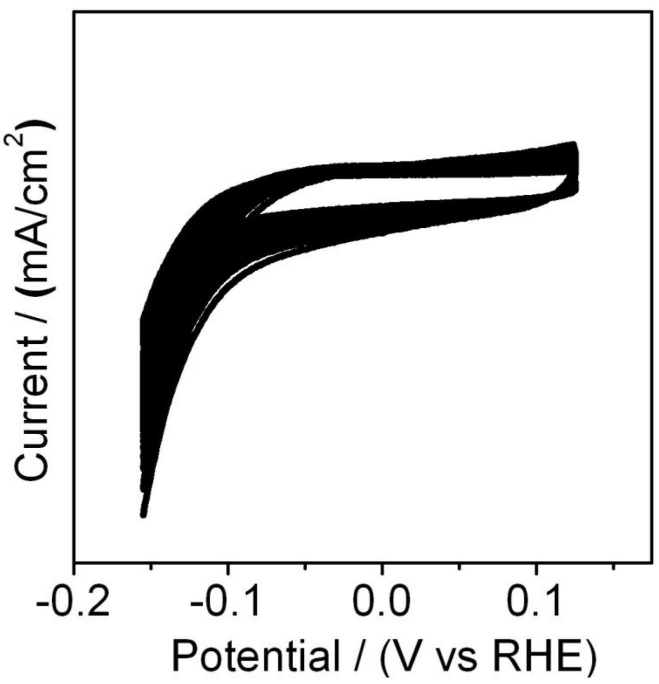

Figure S3. The CV image for 1000 cycles.

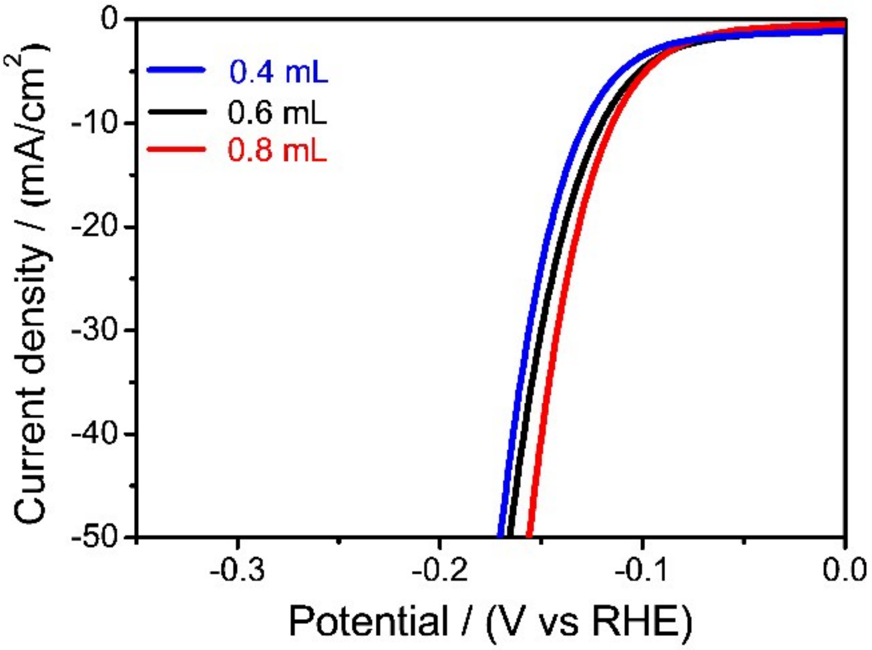

Figure S4. The polarization curves with different GO concentration of $Fe_{0.86}Co_{0.14}S_2$/RGO.

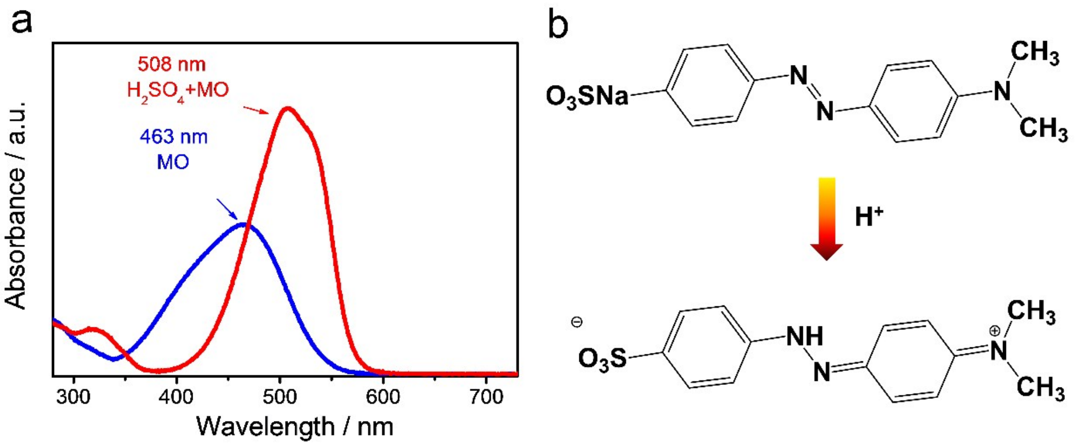

Figure S5. (a) The UV-visible adsorption change of MO in neutral and acidic solution. (b) The structure change of MO with the increase of acidity.

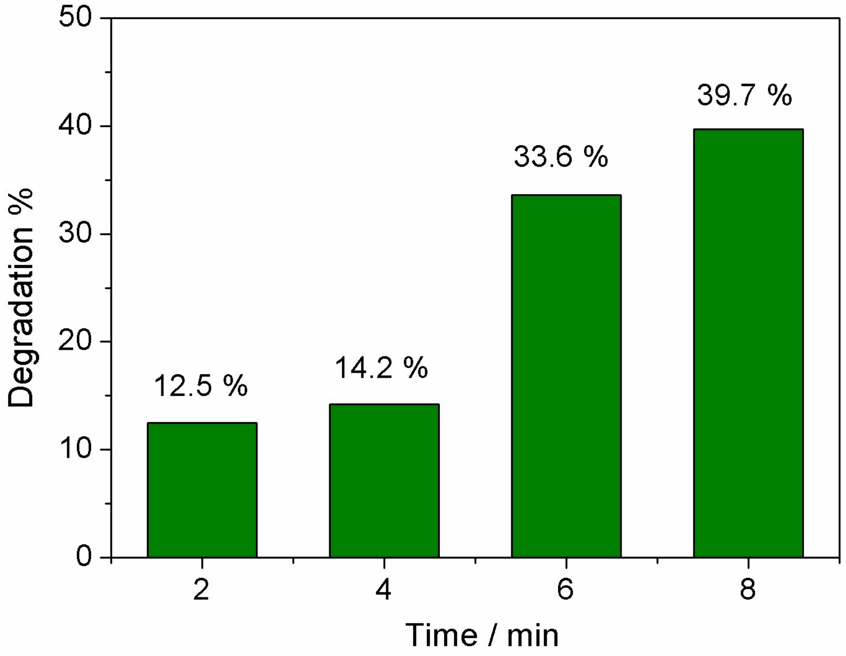

Figure S6. The degradation rate at different time intervals.

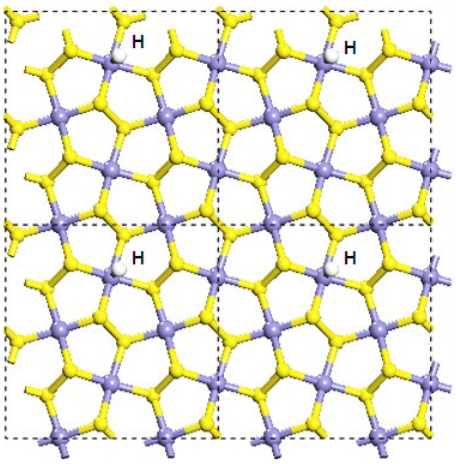

Figure S7. Top view of the upper three atomic layer of FeS_2 (100) surface with atomic H adsorption at Fe_{4c} site.

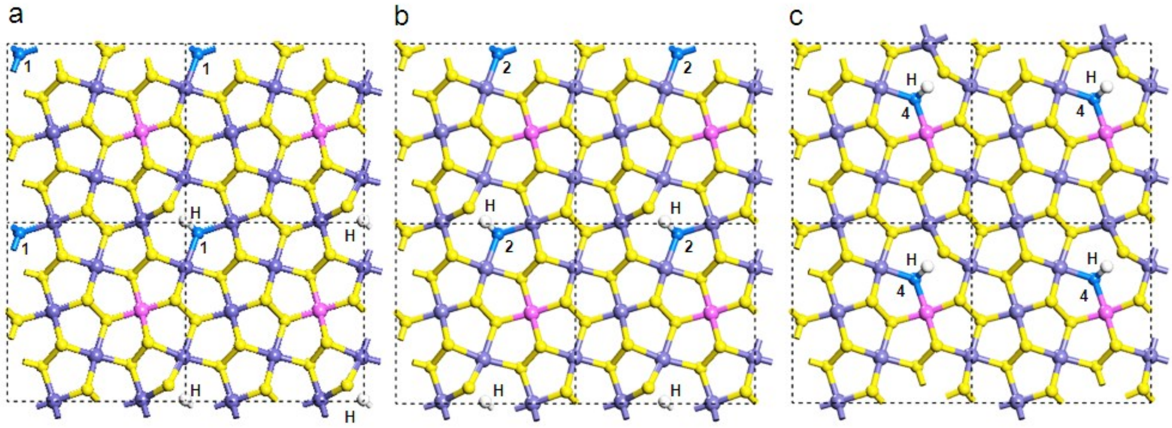

Figure S8. Top view of the upper three atomic layer of $Fe_{0.875}Co_{0.125}S_2$ (100) surface with atomic H adsorption at S_{4c}-1 (a), S_{4c}-2 (b) and S_{4c}-4 (c) sites. As there are too many S atoms, target S atoms are marked with blue color to be easy captured.

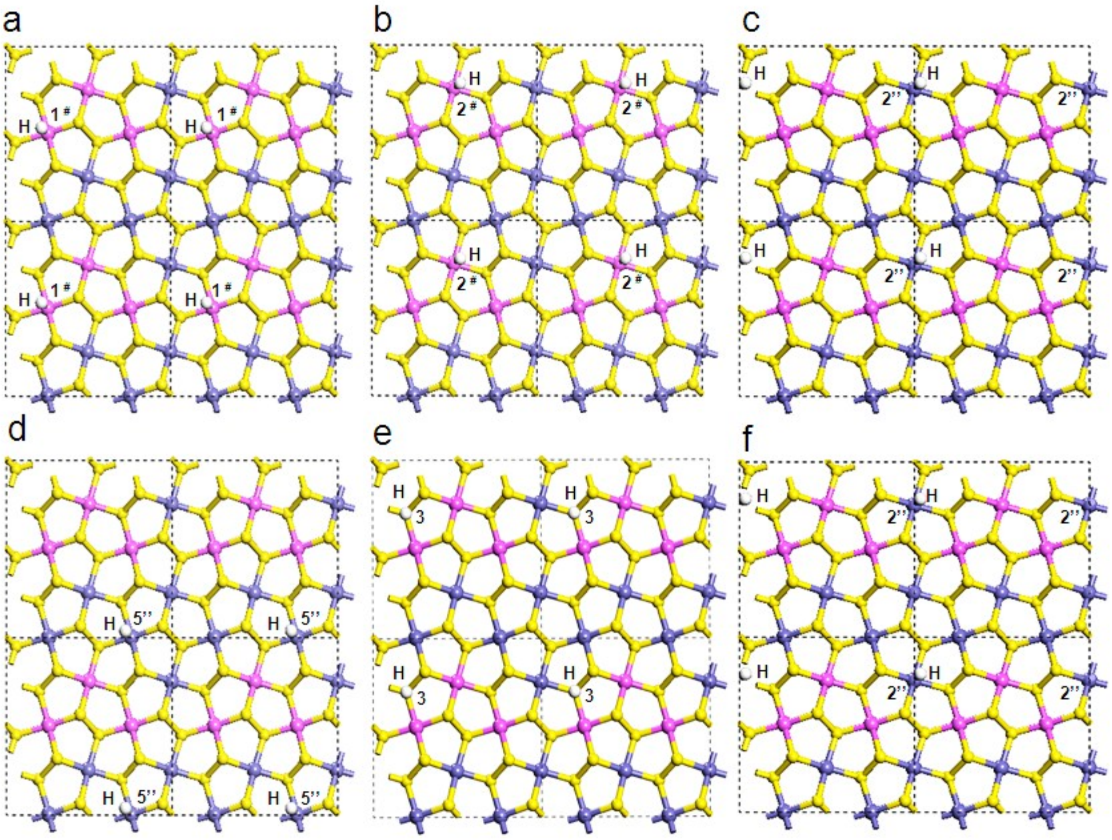

Figure S9. Top view of the upper three atomic layer of $Fe_{0.625}Co_{0.375}S_2$ (100) surface with atomic H adsorption at Co_{4c}-1$^{\#}$ (a), Co_{4c}-2$^{\#}$ (b), Fe_{4c}-1'' (c), Fe_{4c}-5'' (d), S_{4c}-3 (unrelaxed) (e) and S_{4c}-3 (relaxed) (f) sites. Among them, the original top view of $Fe_{0.625}Co_{0.375}S_2$ (100) surface with atomic H adsorption at S_{4c}-3 should be identical with (e), which is the prime calculation model. While through the optimization, the H atom migrate from the S_{4c}-3 to Fe_{4c}-1, which bring about Figure f.

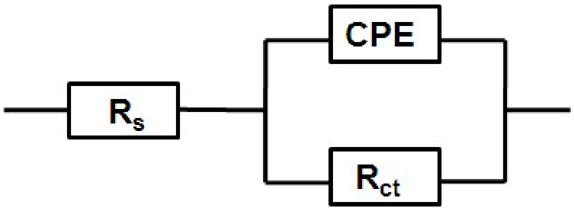

Figure S10. The equivalent circuit model used to fit the experimental data.

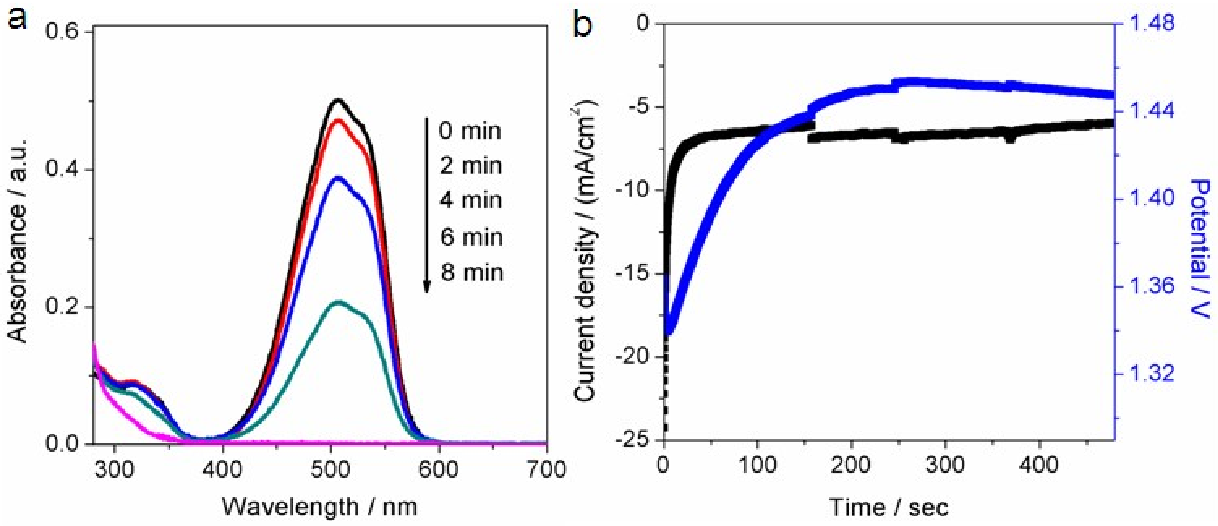

Figure S11. (a) The intensity changes of UV adsorption about MO during different degradation time, 0 min, 2 min, 4 min, 6 min and 8 min with the addition of ter-butanol. (b) Combination of time-dependent current density curve on cathode and the degradation potential on anode of MO degradation process with the addition of ter-butanol.

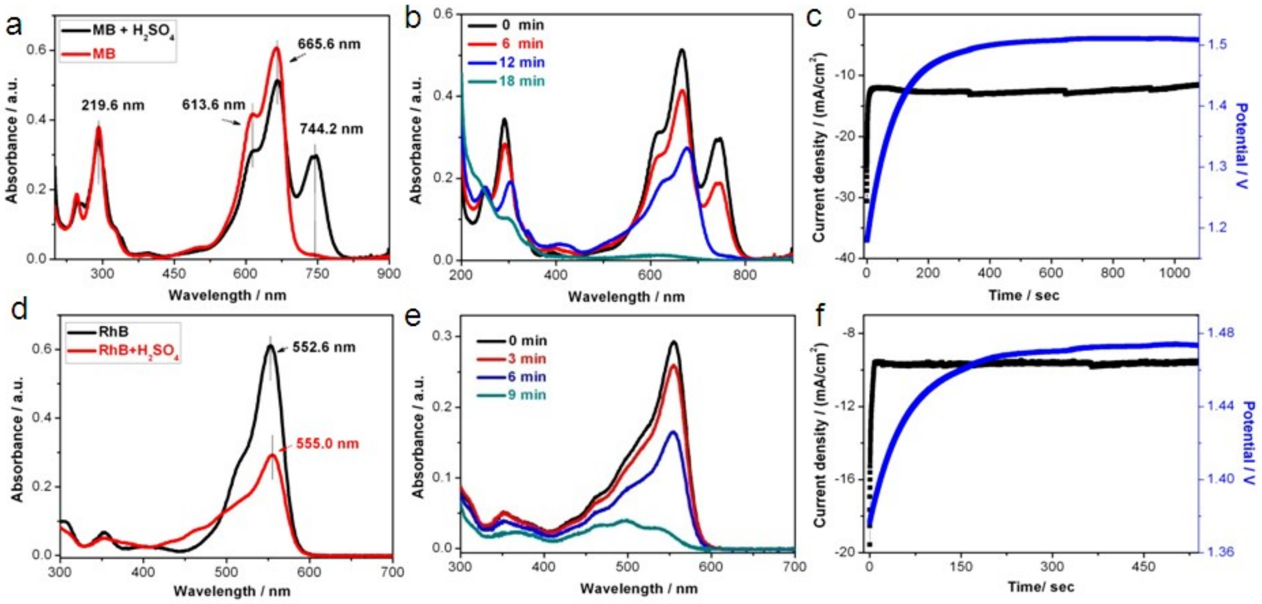

Figure S12. (a) The UV adsorption change of MB in neutral and acidic solution. (b) The intensity changes of UV adsorption about MB during different degradation time, 0 min, 6min, 12 min, 18 min. (c) Combination of time-dependent current density curve on cathode and the degradation potential on anode of MB degradation process. (d)The UV adsorption change of RhB in neutral and acidic solution. (e) The intensity changes of UV adsorption about RhB during different degradation time, 0 min, 3min, 6 min, 9 min. (f) Combination of time-dependent current density curve on cathode and the degradation potential on anode of RhB degradation process.

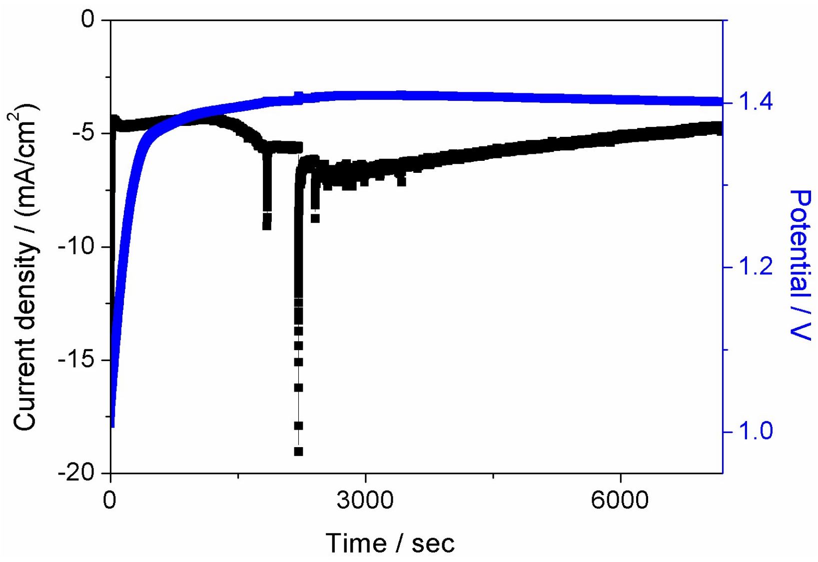

Figure S13. Combination of time-dependent current density curve on cathode and the degradation potential on anode of the industry wastewater degradation process.

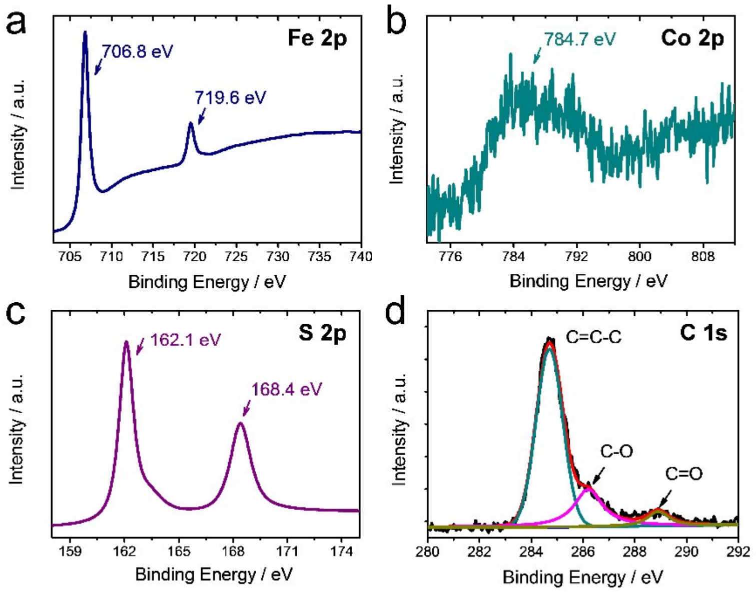

Figure S14. XPS spectra of Fe 2p, Co 2p, S 2p and C 1s from $Fe_{0.86}Co_{0.14}S_2$/RGO.

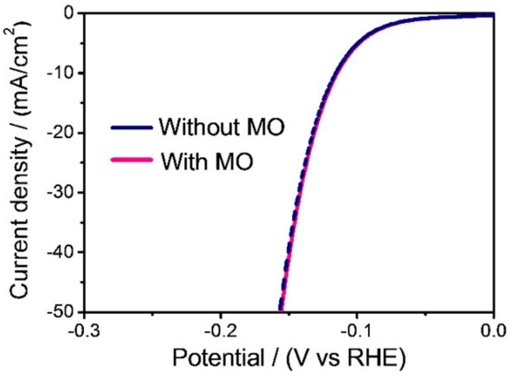

Figure S15. Polarization curves $Fe_{0.86}Co_{0.14}S_2$/RGO in electrolyte with or without MO.

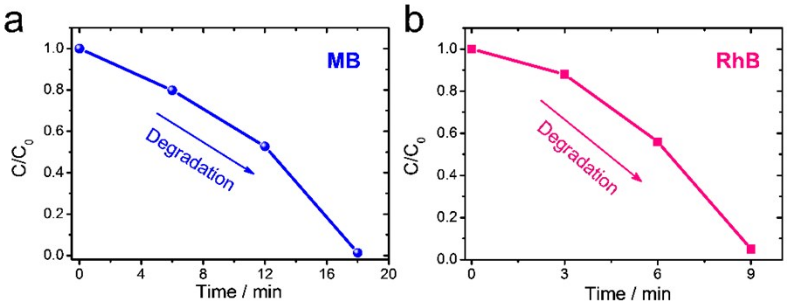

Figure S16. Overall degradation trends of MB and RhB.

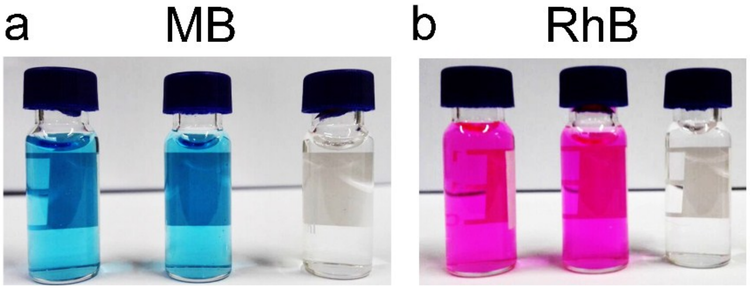

Figure S17. (a) The color changes of MB, MB (H^+) and after degradation. (b) The color changes of RhB, RhB (H^+) and after degradation.

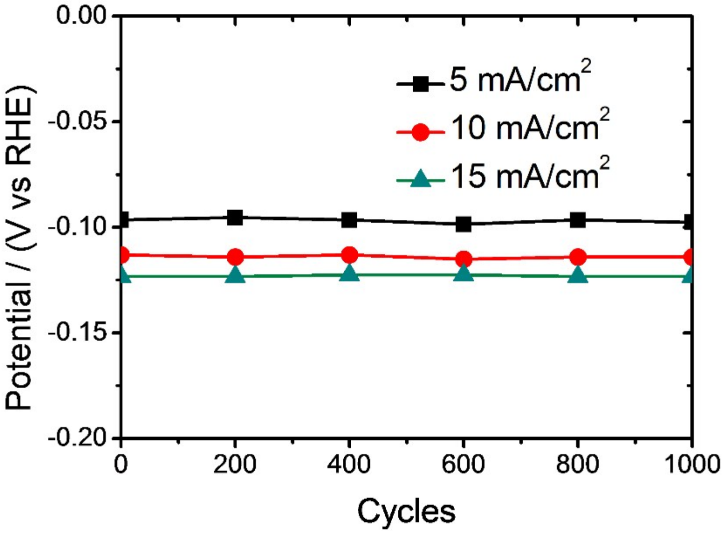

Figure S18. Potential values from the polarization curves of $Fe_{0.86}Co_{0.14}S_2$/RGO recorded initially and after every 200 CV sweeps at 5 mA cm^{-2}, 10 mA cm^{-2}, and 15 mA cm^{-2}, respectively.

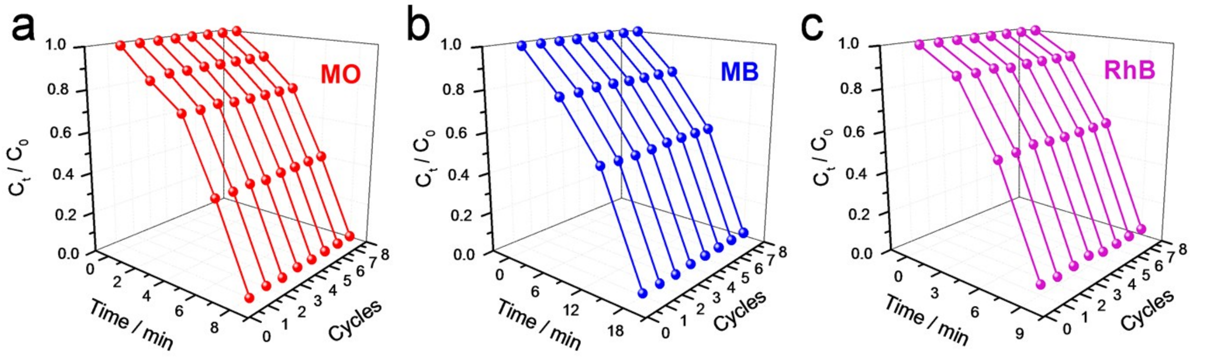

Figure S19. Eight successive degradation curves of MO (a), MB (b) and RhB (c) on anode.

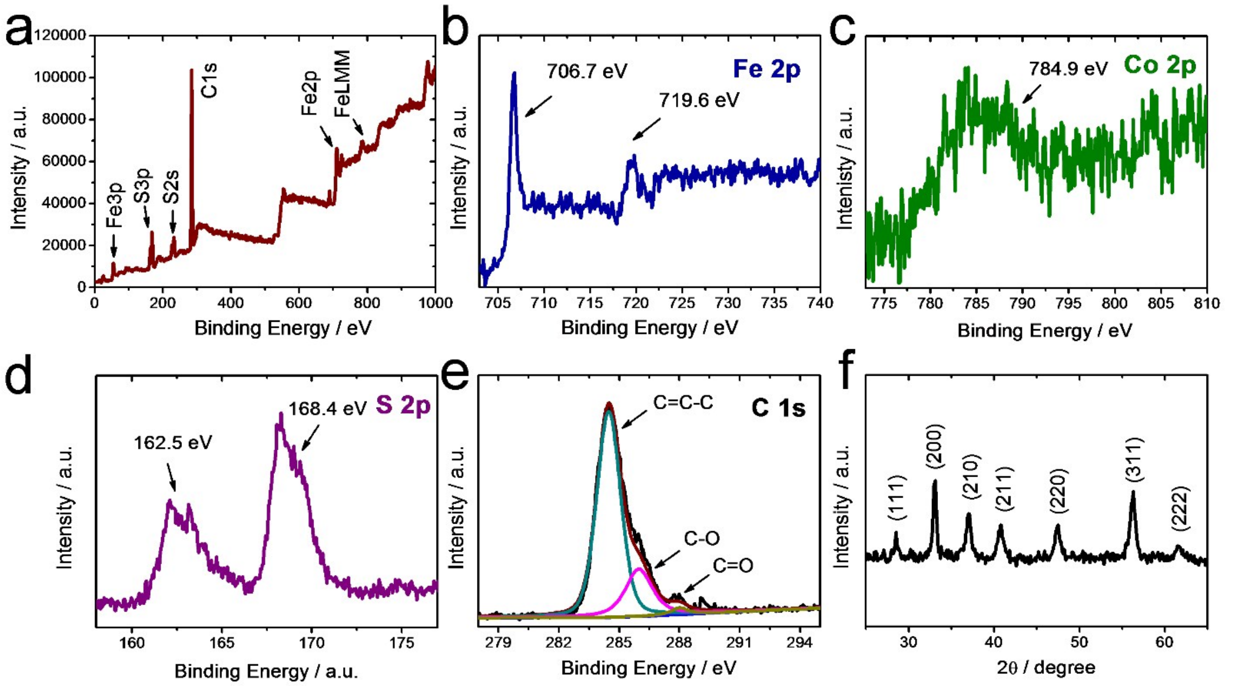

Figure S20. XPS spectra of the reacted $Fe_{0.86}Co_{0.14}S_2$/RGO: (a) XPS full spectrum; (b) Fe 2p spectrum; (c) Co 2p spectrum; (d) S 2p spectrum; (e) C 1s spectrum. (f) XRD pattern of the reacted $Fe_{0.86}Co_{0.14}S_2$/RGO.

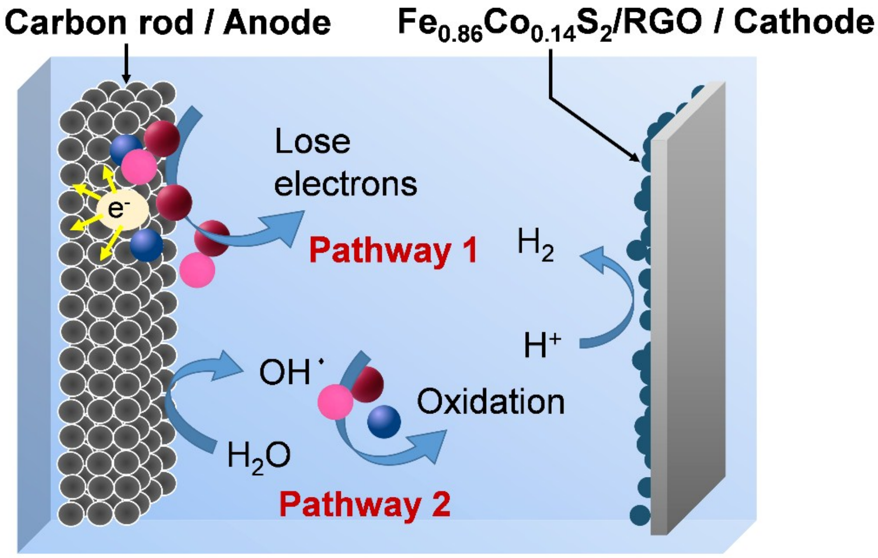

Figure S21. Mechanism illustration of organic dye molecules on anode (carbon rod).

Table S1. Calculated absorption energies of atomic H towards the FeS$_2$ (100) surface, Fe$_{0.875}$Co$_{0.125}$S$_2$ (100) surface and Fe$_{0.625}$Co$_{0.375}$S$_2$ (100) surface and the corresponding △G$_H$.

Pristine FeS$_2$ (100)			**Fe$_{0.875}$Co$_{0.125}$S$_2$ (100)**			**Fe$_{0.625}$Co$_{0.375}$S$_2$ (100)**		
Adsorb-site	Ead	△GH	Adsorb-site	Ead	△GH	Adsorb-site	Ead	△GH
			Co$_{4c}$	-0.69	-0.49	**Co$_{4c}$-1$^{\#}$**	**0.23**	**0.43**
						Co$_{4c}$-2$^{\#}$	**0.24**	**0.44**
						Co$_{4c}$-3$^{\#}$	0.68	0.88
Fe$_{4c}$	**-0.71**	**-0.51**	Fe$_{4c}$	-0.62	-0.42	**Fe$_{4c}$-1”**	**1.18**	**0.47**
						Fe$_{4c}$-2”	0.74	0.94
						Fe$_{4c}$-3”	1.12	1.32
						Fe$_{4c}$-4”	1.12	1.32
						Fe$_{4c}$-5”	**0.28**	**0.48**
S$_{3c}$	0.84	1.04	S$_{3c}$-1’	0.18	0.38	S$_{3c}$-1’	0.81	1.01
			S$_{3c}$-2’	0.91	1.11	S$_{3c}$-2’	0.83	1.03
			S$_{3c}$-3’	1.00	1.20	S$_{3c}$-3’	0.71	0.91
			S$_{3c}$-4’	0.35	0.55	S$_{3c}$-4’	0.79	0.99
			S$_{3c}$-5’	0.44	0.64	S$_{3c}$-5’	0.73	0.93
			S$_{3c}$-6’	0.95	1.15	S$_{3c}$-6’	0.68	0.88
			S$_{3c}$-7’	0.04	0.24	S$_{3c}$-7’	0.82	1.02
			S$_{3c}$-8’	0.74	0.94	S$_{3c}$-8’	0.90	1.10
S$_{4c}$	0.62	0.82	**S$_{4c}$-1**	**-0.23**	**-0.03**	S$_{4c}$-1	0.43	0.63
			S$_{4c}$-2	**-0.20**	**0.00**	S$_{4c}$-2	0.62	0.82
			S$_{4c}$-3	-0.61	-0.41	**S$_{4c}$-3**	**0.27**	**0.47**
			S$_{4c}$-4	**-0.28**	**-0.08**	S$_{4c}$-4	0.65	0.85
			S$_{4c}$-5	-0.50	-0.30	S$_{4c}$-5	0.65	0.85
			S$_{4c}$-6	-0.64	-0.44	S$_{4c}$-6	0.72	0.92
			S$_{4c}$-7	-0.60	-0.40	S$_{4c}$-7	0.96	1.16
			S$_{4c}$-8	-0.38	-0.18	S$_{4c}$-8	0.68	0.88

* Theoretical atomic layer simulations expressed in bold have been depicted in the supporting information.

Table S2. The detailed ingredients analysis of the industry wastewater

Item	Indicator
Appearance	Magenta
Benzoquinone derivative %	3
Tar %	5
Benzoic acid %	0.5
Benzene derivatives (mainly benzene compound)	1.5
COD mg/L	25000
Sulfuric acid %	30~40